EurJIC
European Journal of Inorganic Chemistry

A Journal of
ChemPubSoc Europe

Accepted Article

Title: Versatility of terpyridine functionalised aryl tetrazoles: photophysical properties, ratiometric sensing of zinc cations and sensitisation of lanthanide luminescence

Authors: Phillip Wright, Jacek Kolanowski, Filipek Wojciech, Evan Moore, Stefano Stagni, Elizabeth New, and Massimiliano Massi

To be cited as: *Eur. J. Inorg. Chem.* 10.1002/ejic.201700663

Link to VoR: http://dx.doi.org/10.1002/ejic.201700663

WILEY-VCH

10.1002/ejic.201700663

Versatility of terpyridine functionalised aryl tetrazoles: photophysical properties, ratiometric sensing of zinc cations and sensitisation of lanthanide luminescence

Phillip J. Wright,[a] Jacek L. Kolanowski,[b] Wojciech Filipek,[b] Evan G. Moore,[c] Stefano Stagni[d,]*, Elizabeth J. New,[b,]* Massimiliano Massi[a,]*

[a] Curtin Institute of Functional Materials and Interfaces - Department of Chemistry, Curtin University, WA 6102, Australia.

[b] School of Chemistry, The University of Sydney, NSW 2006, Australia.

[c] School of Chemistry and Molecular Biosciences, University of Queensland, QLD 4072, Australia.

[d] Department of Industrial Chemistry "Toso Montanari" - University of Bologna, Bologna 40136, Italy.

Abstract

Four new tetrazole-containing species in conjugation with terpyridine moieties *via* a phenyl or pyridyl linker have been synthesised and characterised. In the series, the tetrazole funcational groups are either in their acidic form or alkylated at the N2 position with a methyl group. The photophysical properties of the species revealed moderate UV or efficient blue fluorescent emission, with photoluminescence quantum yields around 30% and 80% for UV and blue emission, respectively. The spectral profiles could be reversibly modulated *via* protonation/deprotonation, with changes consistent with an increase in the electron density on the tetrazole ring upon deprotonation or lowering of the electron density on the terpyridine *via* protonation. The tetrazole-containing species were also investigated for the fluorescent

sensing of biologically and environmentally important metal ions, highlighting a ratiometric response to the presence of Zn^{2+}. Furthermore, this ratiometric response could be well discriminated from that of interfering Cd^{2+} ions. Lastly, the species have been investigated as ligands for Eu^{3+} and Yb^{3+} cations, revealing efficient sensitisation to give typical red and near infrared emission, respectively.

Introduction

As a functional group, tetrazoles have found widespread use in the design of molecular species for diverse applications, including medicinal chemistry,[1] coordination polymers,[2] crystal growth inhibition[3] and luminescent materials.[4-6] Tetrazoles are five-membered aromatic heterocycles possessing four adjacent N atoms. In terms of acidity, tetrazoles have pK_a values similar to carboxylic acids, so negatively charged tetrazolates are easily accessible *via* deprotonation reactions.[7,8] For this reason, tetrazoles are considered to be more metabolically stable bioisosteres of carboxylic acids.[9] The presence of four sp^2-hybridised lone pairs on the nitrogen atoms allows the construction of complex molecular architectures *via* bridging multiple metal ions,[2] and many of these examples have been reported for species containing both transition metals and lanthanide elements.[10-15]

In the area of luminescent metal complexes, tetrazoles have proven to very versatile ligands, both from the point of view of coordination modes and modulation of photophysical properties. We have been interested in this area for some time, highlighting the construction of multinuclear luminescent assemblies with metallic cations such as Re(I),[16] Ir(III),[5] Ru(II),[12] Cu(I)[17] and Pt(II).[18] Furthermore, we have shown how coordinated tetrazoles can undergo facile reaction with electrophilic reagents, thus modulating the photophysical properties of the complex.[19] These complexes have proven to be useful

10.1002/ejic.201700663

in applications such as organic light emitting devices[20] and molecular probes for live cell imaging.[21] In these studies, the luminescent properties mainly originate from the final metal complex rather than the tetrazole-containing ligands.

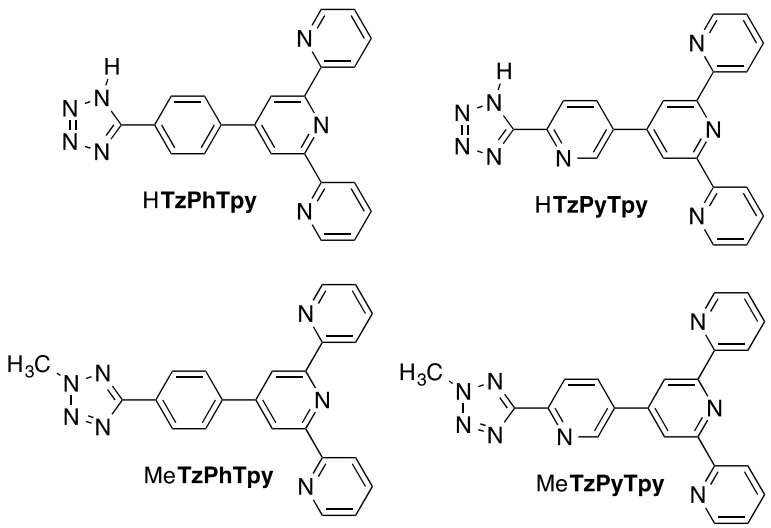

Figure 1. Terpyridine functionalised tetrazole species investigated in this work.

In trying to expand the scope of tetrazole-containing species for luminescent applications, we have decided to investigate molecular architectures composed of a tetrazole functional group conjugated to a terpyridine moiety *via* either a phenyl or pyridyl linker. The rationale for the design of this series (Figure 1) was to access ligands with intrinsic photophysical properties that could be modulated *via* reversible interaction with electrophiles and Lewis acids, as well as complexation with transition and lanthanide metal cations. In the newly synthesised compounds, the tetrazole functional groups are either in their acid form or alkylated with a methyl substituent at the N2 position. This work reports the synthetic protocols for the construction of the terpyrdine-functionalised tetrazoles shown in Figure 1, along with the investigation of their intrinsic photophysical properties and their sensitivity to

protonation/deprotonation reactions. Furthermore, the versatility of these species for luminescent applications are highlighted in the ratiometric sensing of Zn^{2+} cations, with discrimination of interference from Cd^{2+} cations, as well as sensitisation of visible red emission and near-infrared emission *via* complexation with Eu^{3+} and Yb^{3+}, respectively.

Results and Discussion

Synthesis and spectroscopic characterisation

Following a published procedure,[22] the precursor NC**PhTpy** was prepared by reaction of 4-cyanobenzaldehyde and pyridine-2-carboxyaldehyde in ethanol and in the presence of potassium hydroxide and aqueous ammonia. The targeted species H**TzPhTpy** was then prepared *via* 1,3-dipolar cycloaddition between sodium azide and NC**PhTpy** in toluene (Figure 2), following slight modifications of a reported procedure.[23]

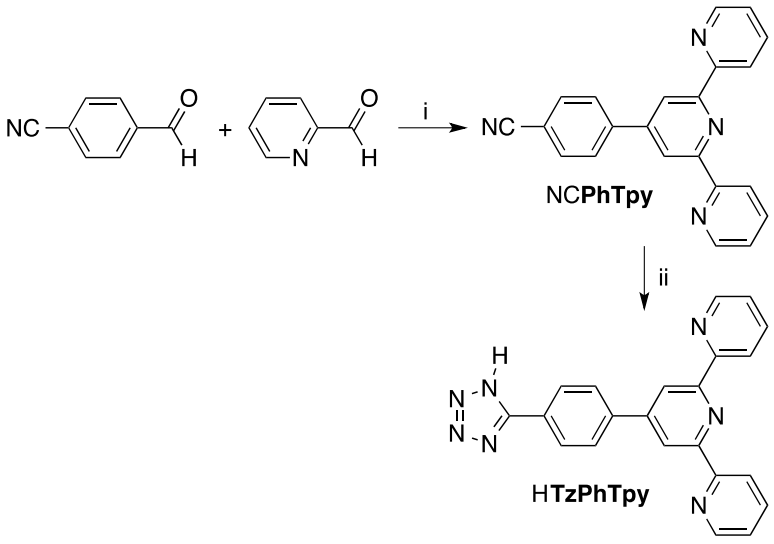

Figure 2. Synthesis of the ligand H**TzPhTpy**. Reagents and conditions: i) KOH, NH_4OH, EtOH, 18 h, rt; ii) $Et_3N{\cdot}HCl$, NaN_3, toluene, 18 h, reflux.

H**TzPhTpy** was characterised by IR, ^{1}H-NMR and ^{13}C-NMR spectroscopy. The IR spectrum displays a band at 1603 cm^{-1}, corresponding to the CN stretch of the tetrazole moiety, and the spectrum was absent of a nitrile peak at 2225 cm^{-1}, indicating absence of starting material.

Due to the low solubility of this compound in common deuterated solvents and the presence of multiple overlapping peaks, the ^{1}H-NMR spectrum of H**TzPhTpy** was difficult to interpret (Figure S1). The spectrum in deuterated DMSO shows broad signals between 8.80-8.95 ppm, 8.20-8.35 ppm, and 7.67-7.76 ppm, with integration ratio of 6:6:2, matching the proposed structure. Excess triethylamine was therefore added to the deuterated DMSO solution to promote the formation of the more soluble triethylammonium tetrazolate salt [HNEt$_3$][**TzPhTpy**]. The resulting ^{1}H-NMR spectrum (Figure S1) becomes more defined, showing as expected seven peaks appearing in the aromatic region between 9.00 and 7.00 ppm, belonging to the phenyl and pyridine rings. The ^{13}C-NMR spectrum for this compound exhibits thirteen signals corresponding to those expected for the product. In particular, the formation of the tetrazole ring is supported by the presence of a peak at 160.3 ppm.[24,25]

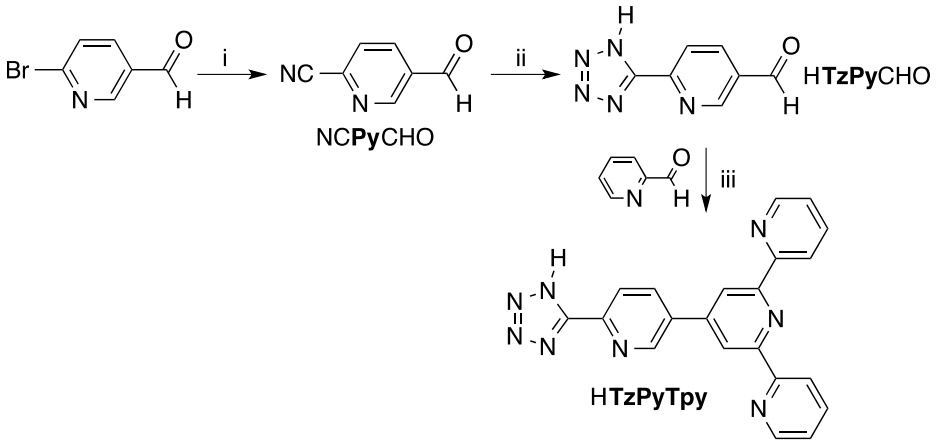

Figure 3. Synthesis of the ligand H**TzPyTpy**. Reagents and conditions: i) CuCN, DMF, 4 h, 120 °C; ii) Et$_3$N·HCl, NaN$_3$, toluene, 18 h, reflux; iii) KOH, NH$_4$OH, EtOH, 18 h, rt.

An alternative sequence was followed for the preparation of H**TzPyTpy** (Figure 3). Firstly, 2-cyanopyridine-5-carboxyalhedyde, NC**Py**CHO, was prepared by reaction of 2-bromopyridine-5-carboxyalhedyde with copper(I) cyanide in DMF, according to a previously published procedure.[26] A 1,3-dipolar cycloaddition reaction was then performed on NC**Py**CHO for the formation of the tetrazole ring in H**TzPy**CHO.[23] The species H**TzPy**CHO was analysed by IR, ^{1}H-NMR, and ^{13}C-NMR spectroscopy. The IR spectrum for this compound has key signals at 1704 cm^{-1}, corresponding to the aldehyde carbonyl group, and 1605 cm^{-1} for the tetrazole CN stretch.

The ^{1}H-NMR spectrum matches the desired product, showing a singlet at 10.20 ppm corresponding to the H atom of the CHO substituent, along with one singlet and two doublets belonging to the three H atoms of the pyridine ring. The ^{13}C-NMR spectrum displays seven signals consistent with the proposed structure, with noteworthy resonances at 191.8 ppm, corresponding to the aldehyde C atom, and 154.6 ppm, corresponding to the tetrazolic C atom.[24,25]

The terpyridine moiety was formed by reaction of H**TzPy**CHO with pyridine-2-carboxyaldehyde in ethanol and in the presence of potassium hydroxide and aqueous ammonia.[22] The product was characterised by IR spectroscopy and showed a signal at 1597 cm^{-1}, corresponding to the tetrazole CN stretch. The product was also characterised by ^{1}H-NMR spectroscopy after the addition of excess triethylamine (Figure S2) to display better resolved peaks, as in the previous case of H**TzPhTpy**.

Alkylation of the tetrazole ring in H**TzPhTpy** was first attempted by reaction with trifluoroacetic acid and sulfuric acid in *tert*-butanol. This procedure was chosen since its regioselectivity for the N2 position of the tetrazole ring was previously demonstrated.[27,28] However, this reaction failed to yield the target alkylated species. Therefore, H**TzPhTpy** was treated with methyl iodide and potassium carbonate in acetonitrile at reflux. These conditions allowed the isolation of a mixture of methylated regioisomers at

the N1 and N2 position of the tetrazole ring, with an approximate ratio of 4:6, respectively, evidenced by NMR analysis. The two regioisomers could be easily separated *via* column chromatography. The identity of Me**TzPhTpy** was confirmed by the appearance of a singlet corresponding to three H atoms at 4.42 ppm in the ^{1}H-NMR spectrum, belonging to the methyl substituent (Figure S3). Furthermore, the resonance at 165.0 ppm belonging to the tetrazolic C atom in the ^{13}C-NMR spectrum confirmed the methylation at the N2 atom of the tetrazole ring.[24,25]

To install a consistent alkylating functional group bound to the tetrazole ring, the same methylation protocol was applied to H**TzPyTpy**. The analysis at the end of the reaction by NMR revealed the expected mixture of regioisomers in a 6:4 ratio for the N1 and N2 methylated products, respectively. Unfortunately, these could not be separated by column chromatography. A new synthetic strategy was therefore adopted for the preparation of Me**TzPyTpy** (Figure 4). Firstly, the previously prepared 2-(1H-tetrazol-5-yl)pyridine-5-carboxyaldehyde, H**TzPy**CHO, was methylated by reaction with methyl iodide and potassium carbonate. The methylation yielded a 4:6 mixture of N1 and N2 alkylated regioisomers, which could be easily purified by column chromatography. Then, the isolated Me**TzPy**CHO was reacted with pyridine-2-carboxyaldehyde, potassium hydroxide, and aqueous ammonium hydroxide to yield the targeted terpyridine functionalised species Me**TzPyTpy**.[22] The presence of a singlet at 4.49 ppm for the methyl substituent in the ^{1}H-NMR spectrum confirmed the identity of the target compound (Figure S4), whereas the N2 isomer was determined by the resonance of the tetrazolic C atom at 164.8 ppm in the ^{13}C-NMR spectrum.[24,25]

10.1002/ejic.201700663

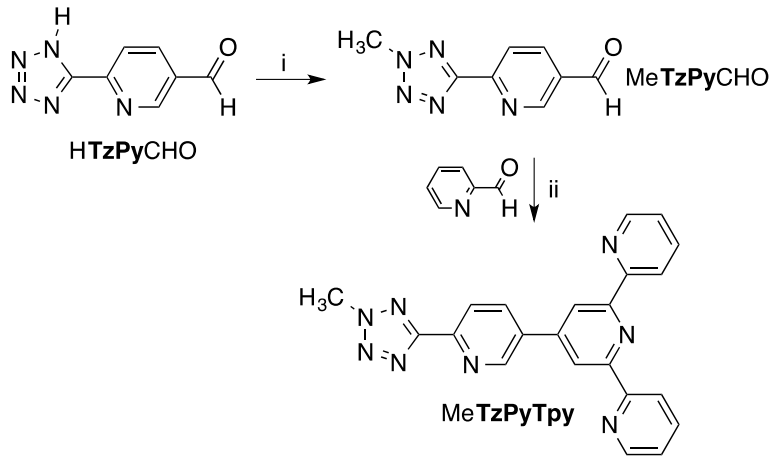

Figure 4. Synthetic procedure for the preparation of Me**TzPyTpy**. Reagents and conditions: i) CH_3I, K_2CO_3, CH_3CN, 12 h, reflux; ii) KOH, NH_4OH, EtOH, 18 h, rt.

Photophysical properties

A summary of the photophysical properties of H**TzPhTpy**, H**TzPyTpy**, Me**TzPhTpy**, and Me**TzPyTpy** recorded in acetonitrile is reported in Table 1. The absorption profiles of the four species (Figure 5) highlight the presence of intense and structured bands in the region between 200 and 350 nm. These bands are mainly ascribed to spin-allowed π-π^* transitions with possible admixtures of n-π^* transitions in the lower energy region of the broad bands. The lowest energy shoulders appear red-shifted for H**TzPhTpy** and H**TzPyTpy** when compared to the two methylated species Me**TzPhTpy** and Me**TzPyTpy**.

Table 1. Photophysical properties from acetonitrile solutions (*ca* 10^{-5} M).

Compound	Absorption	Emission (298 K)		
	λ ($10^4\varepsilon$) [nm] ([$M^{-1}cm^{-1}$])	λ [nm]	τ [ns]	Φ
H**TzPhTpy**	295 (2.06)	426	2.62	0.77
	253 (1.15)			
	231 (1.51)			
H**TzPyTpy**	295 (3.32)	400	3.36	0.85
	253 (2.31)			
	230 (2.16)			
Me**TzPhTpy**	283 (3.93)	356	2.84	0.32
	255 (2.51)			
	232 (1.66)			
Me**TzPyTpy**	282 (2.76)	362	2.76	0.28
	253 (2.44)			

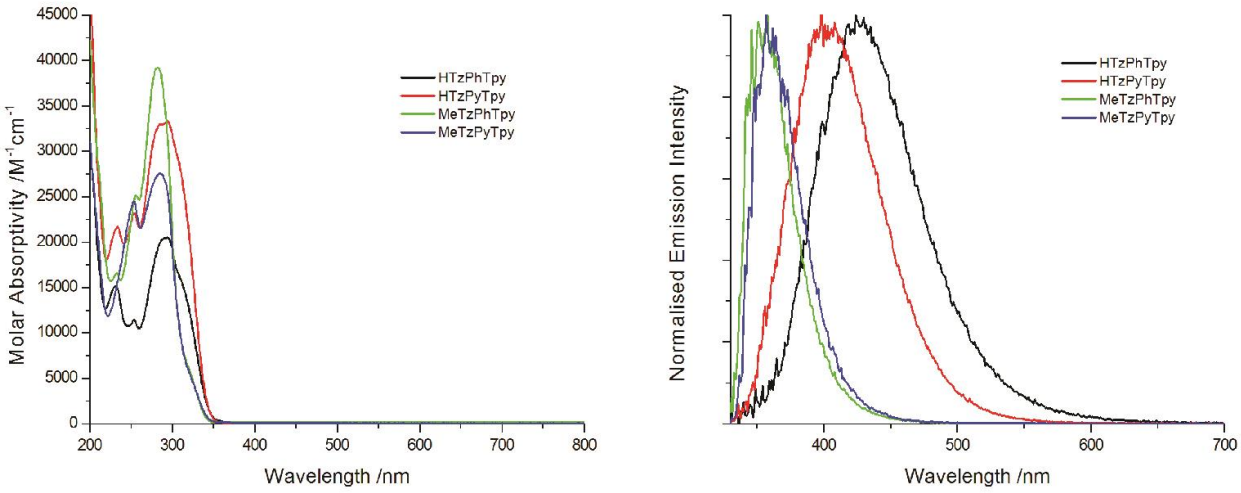

Figure 5. Absorption (left) and emission (right) profiles for the synthesised species from acetonitrile solutions (*ca* 10^{-5} M). The emission spectra were recorded upon excitation at 290 nm.

The emission profiles, shown in Figure 5, display broad bands in the late UV region with similar maxima at 356 and 362 nm for the methylated species Me**TzPhTpy** and Me**TzPyTpy**, respectively. On the other hand, H**TzPhTpy** and H**TzPyTpy** display red-shifted profiles in the blue region, peaking at 426 and 400 nm, respectively. This red-shifted emission might be explained by the more electron-rich nature of the unmethylated tetrazole rings, which could also exist in solution as a zwitterionic form displaying donor-

acceptor behaviour between the anionic tetrazolate ring and cationic protonated form of the terpyridine moiety. This conclusion is also corroborated by the slight blue-shift of H**TzPyTpy** with respect to H**TzPhTpy**, as the presence of the pyridine linker for the former causes a reduction of the electron density of the tetrazole ring *via* charge delocalisation. H**TzPhTpy** and H**TzPyTpy** display strong emission intensity with quantum yield (Φ) values measured at 0.77 and 0.85, respectively. The quantum yield reduces to moderate upon methylation, with values at 0.32 for Me**TzPhTpy** and 0.28 for Me**TzPyTpy**. In all cases, the excited state lifetime decay (τ) is very short, of the order of few nanoseconds, which is consistent with spin-allowed fluorescent emission.

Photophysical changes upon addition of acids and bases

The relative energy of the excited states for the synthesised species can be readily influenced by acid-base equilibria occurring on the tetrazole and terpyridine substituents. To investigate the effect of these equilibria on the luminescent properties, we measured the changes in the absorption and emission spectra upon sequential addition of camphorsulfonic acid in acetonitrile solutions. The methylated species Me**TzPhTpy** and Me**TzPyTpy** were firstly investigated, as this system is absent from the added protonation equilibrium occurring on the tetrazole substituent.

The sequences of absorption and emission plots for acetonitrile solutions of Me**TzPhTpy** and Me**TzPyTpy** are shown in Figure 6, where each sequential spectrum represents an addition of 0.33 equivalents of acid. The trend in the absorption plots is analogous and highlights the progressive appearance of a red-shifted band peaking around 330 nm, and the presence of two isosbestic points in each spectrum. The corresponding emission profiles also show an analogous trend, where the UV emission band

progressively disappears with the concomitant appearance of a broader red-shifted band of aqua-coloured emission for Me**TzPhTpy** and blue emission for Me**TzPyTpy**. This trend is rationalised by protonation occurring at the terpyridine substituent causing a stabilisation of the π^* orbitals. The effective result is a reduction of the HOMO-LUMO gap. The blue shifted emission for the protonation of Me**TzPyTpy**, with respect to Me**TzPhTpy**, is rationalised by the fact that the protonation can also occur at the 2-pyridyltetrazole position, hence stabilising the π orbitals to a greater extent with consequent widening of the HOMO-LUMO gap.

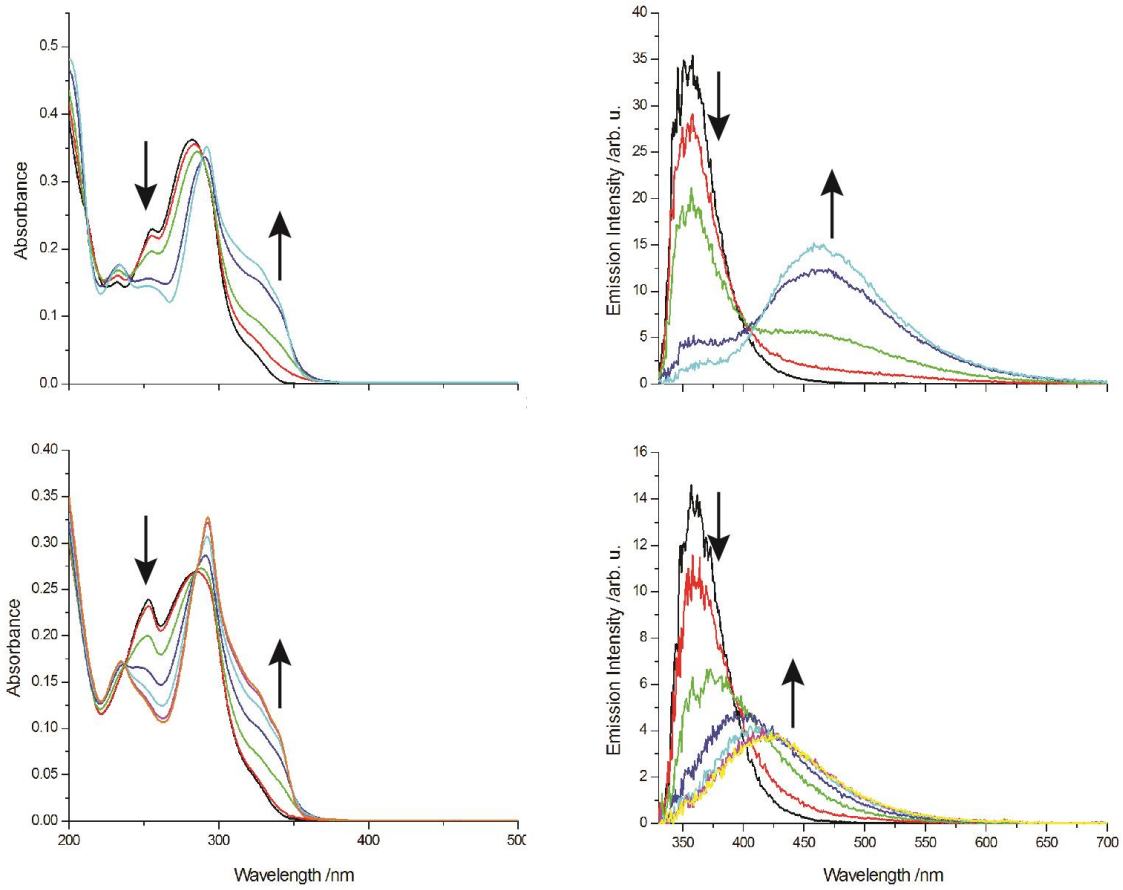

Figure 6. Changes in the absorption and emission spectral profiles for acetonitrile solutions of Me**TzPhTpy** (top) and Me**TzPyTpy** (bottom) upon addition of camphorsulfonic acid. Each sequential line represents an addition of 0.33 equivalents of acid. The starting profile is represented by the black line and the final profile is represented by the light brown line. The emission spectra are recorded upon excitation at 290 nm.

Under similar conditions, the changes in the absorption and emission profiles for H**TzPhTpy** and H**TzPyTpy** were monitored (Figure S5). In this case, the initial spectra were recorded from a solution containing each species and one equivalent of tetrabutylammonium hydroxide to completely deprotonate the tetrazole ring. The profiles highlight changes upon addition of acids, but the resulting spectra resemble a more complex superimposition of bands. The superimposition could originate from protonation occurring on the terpyridine moiety and equilibrating with acid-base equilibria occurring on the tetrazole ring for H**TzPhTpy**, and on the 2-pyridyltetraole site for H**TzPyTpy**. Unlike the methylated derivatives, a clear trend could not be easily established, although significant variations of the absorption and emission spectra are clearly highlighted.

Ratiometric fluorescence sensing of Zn^{2+} and discrimination from Cd^{2+} interference

The pH-induced fluorescence changes of the synthesised tetrazole species and the presence of well-established terpyridine metal-binding motifs prompted us to assess the use of these species for the fluorescent sensing of metal ions. For this investigation, the emission properties were measured in buffered aqueous medium using an excitation wavelength of 290 nm (Figure 7). Similar to the ligands in acetonitrile, the fluorescence spectra in buffered aqueous media highlight broad bands between 350 and 500 nm. The trends in emission maxima are analogous to the previously performed measurements, with a more blue-shifted emission originating from the methylated Me**TzPhTpy** with respect to H**TzPhTpy** and H**TzPyTpy**. The emission profile of Me**TzPyTpy** appears more complex, with the presence of multiple maxima. However, it should be noted that Me**TzPyTpy** exhibits reduced solubility in aqueous

solvent compared to the other three species; hence the spectral profile was measured from non ideal conditions (non transparent solution).

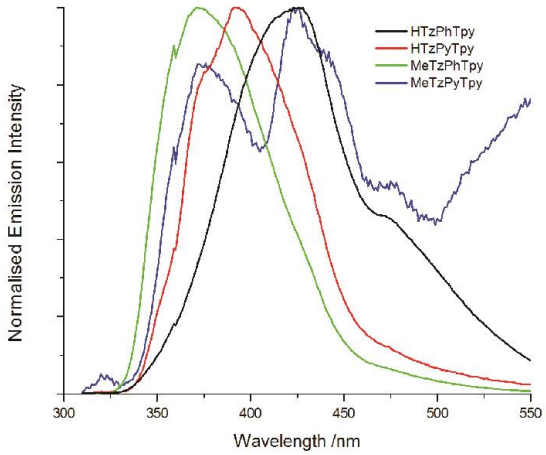

Figure 7. Normalised emission spectra of the aqueous solutions (10 µM in 20 mM HEPES buffer, pH 7.4), recorded with excitation at 290 nm.

The screen of fluorescence responses of the ligands to a wide range of biologically-relevant metal ions revealed that most first row transition metal ions cause quenching of fluorescence (Figure 8). On the other hand, spectroscopically silent alkali and alkali earth cations produce little change in the fluorescent emission of the ligands. In contrast, a unique response of each ligand to Zn^{2+} was observed. A Job's plot analysis of the emission intensity at 380 nm against the molar fraction of Zn^{2+} cations revealed a 2:1 ligand-to-metal binding stoichiometry in the case of Me**TzPyTpy** (Figure S6). This result suggests that the main mode of interaction is through coordination at the terpyridine site. A study of the other ligands was attempted through Job's plots, but the responses were less straightforward to interpret. Zn^{2+} induced a change in the spectral profile of H**TzPhTpy**, with the fluorescence maximum shifting from 410 to 480 nm (Figure 8a). By monitoring the ratio of intensity for the emission at 480 nm and 410 nm, it is

possible to distinguish Zn^{2+} from all other investigated metal ions. Similarly, the addition of Zn^{2+} to H**TzPyTpy** induced a fluorescence increase, as well as the appearance of shoulders at 360 and 480 nm (Figure 8b), which can be used to identify the presence of Zn^{2+} over other metal ions. For Me**TzPhTpy**, addition of Zn^{2+} caused a marked ratiometric change, with a new emission maximum at 500 nm (Figure 8c). The integrated emission intensity at this new peak increases uniquely for Zn^{2+}. The general appearance of red shifted peaks is analogous to the results obtained *via* protonation of the species, and could be ascribed to the coordination of Zn^{2+} to the terpyridine moiety, therefore lowering the energy of delocalised π^* orbitals. Finally, Zn^{2+} alone was found to induce increased emission of the 380 nm peak of Me**TzPyTpy** (Figure 8d).

10.1002/ejic.201700663

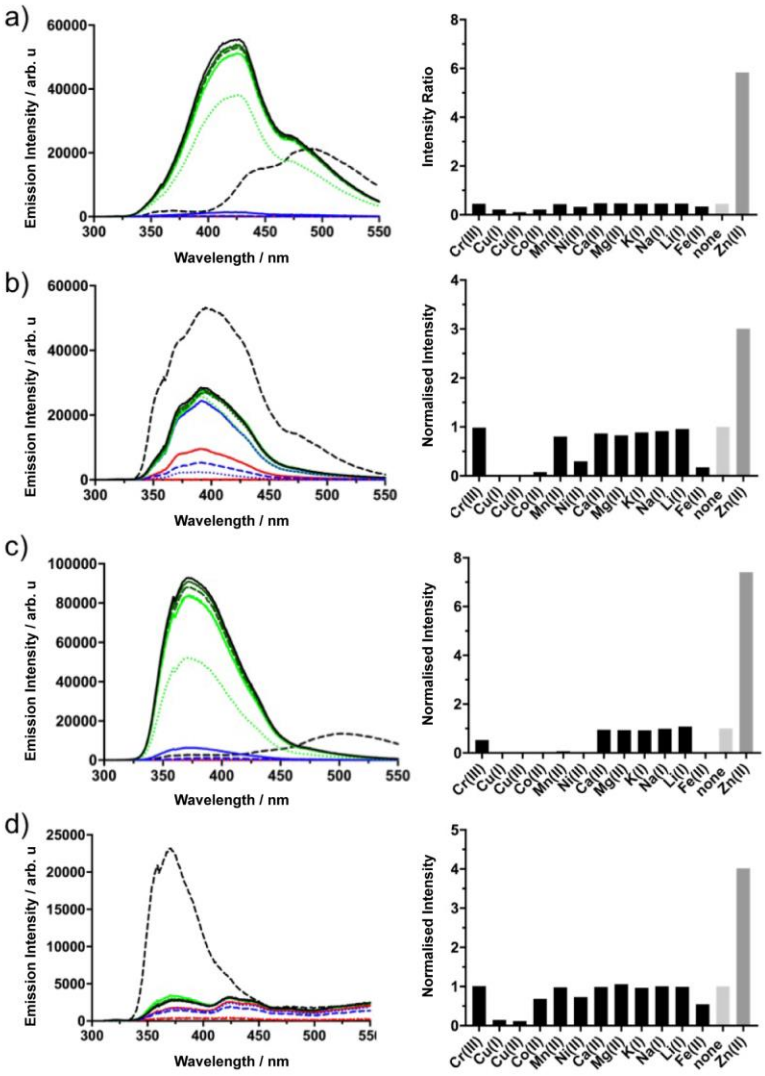

Figure 8. Fluorescent response (excitation at 290 nm) of the solutions (10 µM in 20 mM HEPES buffer, pH 7.4) of (a) H**TzPhTpy**, (b) H**TzPyTpy**, (c) Me**TzPhTpy** (red), (d) Me**TzPyTpy** to biologically relevant metal ions (10 eq): ligands alone (black, solid line), Zn(II) (black, dashed line), Li(I) (dark green, solid), Na(I) (dark green, dashed), K(I) (dark green, dotted), Mg(II) (light green, solid), Ca(II) (light green, dashed), Cr(III) (light green, dotted), Mn(II) (blue, solid), Fe(II) (blue, dashed), Co(II) (blue, dotted), Ni(II) (red, solid), Cu(II) (red, dashed), Cu(I) (red, dotted). Fluorescent spectra (left) and selected parameters (right) - specific for each different ligand - allowing for the distinction of Zn(II) from other metals: (a) fluorescence emission ratio at 480 nm / 410 nm, (b) fluorescence intensity at 360 nm, (c) integrated emission intensity from 500 nm to 550 nm (d) integrated emission intensity from 340 nm to 500 nm.

These results demonstrate the potential of these ligands to act as selective sensors of Zn^{2+}, whether alone or incorporated into more elaborate molecular systems. Furthermore, all ligands exhibit a

ratiometric response to Zn^{2+}, which is a particularly valuable mode of fluorescence sensing as emission ratios are independent of fluorophore concentration and other background parameters.[29] Zinc is an essential metal ion biology, performing a plethora of roles including structure stabilisation, Lewis acid catalysis ,[30] and putative roles in signalling.[31] As a result, there is great interest in detecting this metal ion in cellular studies, and to this end a number of Zn^{2+}-selective sensors have been reported,[32,33] the majority of which are based on ligands bearing pyridyl coordinating motifs, consistent with the findings presented in this work.

A longstanding challenge in the fluorescent sensing of Zn^{2+} is the potential interference from Cd^{2+}, which can induce similar fluorescence changes due to its similar chemical nature.[34] While basal cellular Cd^{2+} levels are not expected to be sufficiently high to interfere with Zn^{2+} sensing in biological studies, Cd^{2+} is itself a highly toxic metal, and the measurement of cellular Cd^{2+} levels in systems potentially subjected to Cd^{2+} exposure is therefore important.[35] Furthermore, since cadmium is widely-used in industry, its unambiguous detection in environmental samples (which are likely to contain considerable background Zn^{2+}) is also essential. We therefore compared the responses of the ligands to Cd^{2+} and Zn^{2+} (Figure 9). When we monitored the response to Cd^{2+} according to the same parameters reported above, we found similar fluorescence changes to those observed for Zn^{2+} (Figure S7). However, Cd^{2+} induced unique spectral changes for H**TzPhTpy**, H**TzPyTpy** and Me**TzPhTpy** (Figure 9a-c). In contrast Me**TzPyTpy** showed the same spectral form in the presence of both Zn^{2+} and Cd^{2+} (Figure 9d). For the former set of ligands, we have therefore been able to identify parameters that enable the unambiguous discrimination of Zn^{2+} from Cd^{2+}. This unique feature of these ligands may enable the development of fluorescent assays for distinguishing Cd^{2+} from Zn^{2+} in complex mixtures, whether industrial, environmental or biological samples.

10.1002/ejic.201700663

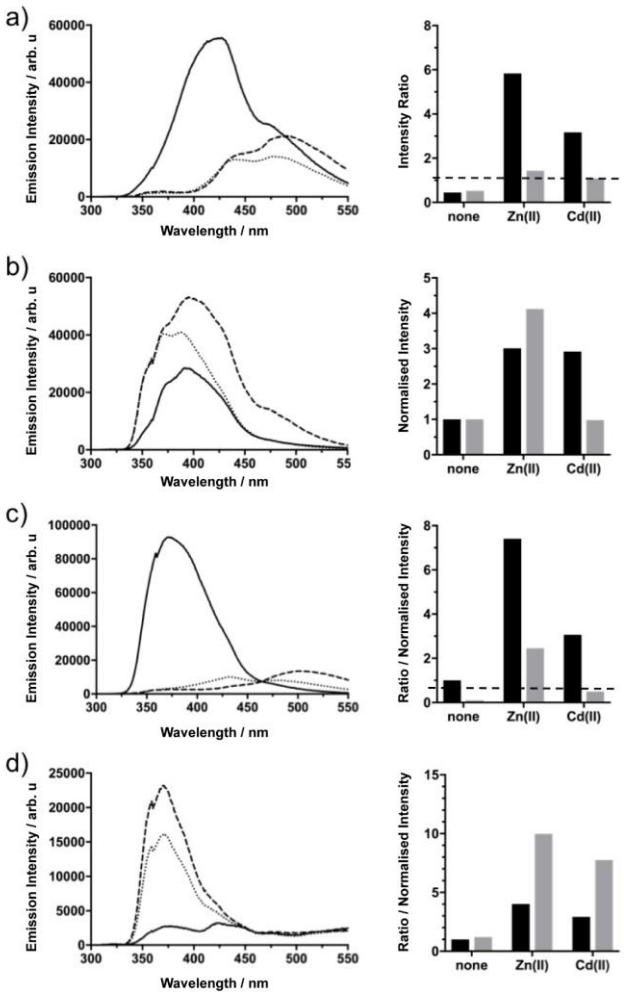

Figure 9. Fluorescent response (excitation at 290 nm) of the solutions (10 µM in 20 mM HEPES buffer, pH 7.4) of (a) H**TzPhTpy**, (b) H**TzPyTpy**, (c) Me**TzPhTpy** (red), (d) Me**TzPyTpy** to 10 eqivalents of Zn(II) and Cd(II). (10 eq) and cadmium. Fluorescent spectra (left panels) of the ligand alone (solid lines) and in the presence of Zn(II) (dashed lines) and Cd(II) (dotted lines). Bar graphs (right panels) represent the selected parameters, which enable the distinction of Zn(II) and Cd(II) from other biologically relevant metals (black bars) and from each other (grey bars, except d), which does not enable the distinction), in particular: a) ratio of fluorescence intensity at 480/410 nm (black) and 480/44 nm (grey) b) normalised intensity of fluorescence at 360 nm (black) and normalised intergrated intensity at 460-560 nm (grey) c) normalised intergrated intensity of fluorescence at λ_{em} 500-550 nm (black) and the ratio of intensities at λ_{em} 525/440 nm (grey) d) normalised intergrated intensity at λ_{em} 340 - 500 nm (black) and the ratio of intensities at λ_{em} 340–400 nm / 500–550 nm (grey). Horizontal dashed lines on the bar graphs represent the threshold value in the case of fluorescence ratios, which enable the distinction of Zn(II) from Cd(II) from other metal ions.

Sensitisation of Eu^{3+} and Yb^{3+} luminescence

The capacity of the synthesised species to sensitise lanthanide luminescence was then explored. As a first step, the relative energy of the triplet $^3\pi$-π^* excited states of the ligands was estimated by adding excess Gd^{3+} in acetonitrile solution.[36] $[Gd(NO_3)_3(DMSO)_n]$ was chosen due to its higher solubility in organic solvents.[37] Figure 10 shows all four absorption profiles after the addition of Gd^{3+}, highlighting the appearance of red-shifted bands around 340 nm, which are ascribed to the complexation of the terpyridine moiety.[4] The emission profiles of these solutions were measured after freezing to 77 K, to enhance the phosphorescent decay from the $^3\pi$-π^* excited states. All the complexes exhibit intense structured bands between 400 and 700 nm, with some residual peaks at wavelengths shorted than 400 nm attributed to residual fluorescent decay from $^1\pi$-π^* excited states (Figure 10). From each of the phosphorescent emission bands, the energies of the 0-0 transitions could be estimated, and the corresponding values are reported in Table 2. From these values, it can be seen that four species could be potential sensitisers for the visible red emission of Eu^{3+} and the NIR emission of Yb^{3+}. For the latter, while the difference in energy between the $^3\pi$-π^* and the Yb^{3+} $^2F_{5/2}$ accepting state is above 10,000 cm^{-1}, a sensitisation mechanism involving a ligand-to-metal charge transfer state with formation of Yb^{2+} could facilitate energy transfer.[38-40]

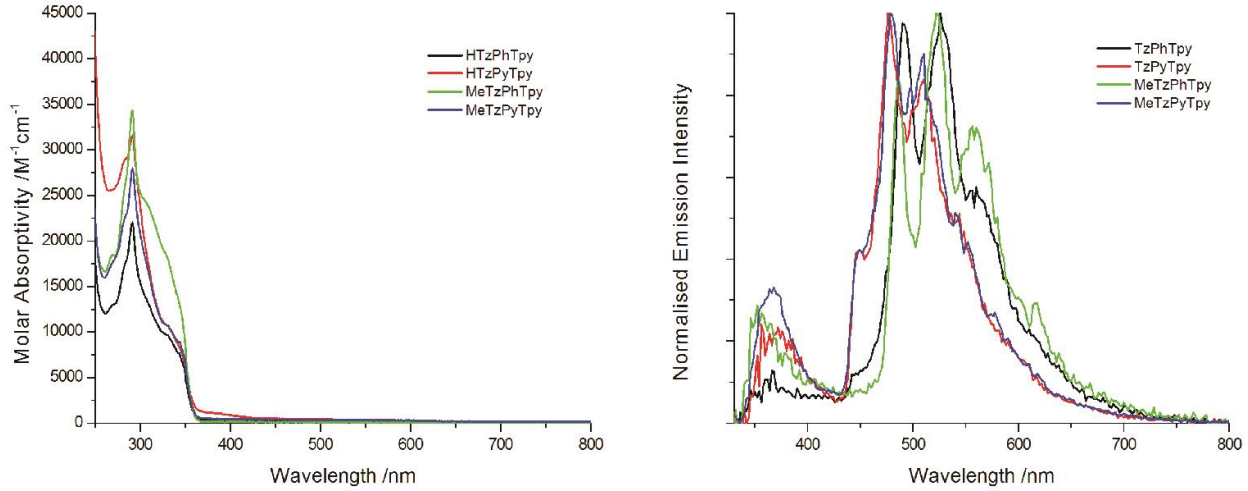

Figure 10. Left: absorption profiles of the synthesised species in the presence of excess Gd^{3+} ions from acetonitrile solutions. Right: Emission profiles ~10^{-5} M acetonitrile solutions of the synthesised species in the presence of excess Gd^{3+} cations at 77 K, with excitation wavelength set at 310 nm.

Table 2. Estimated energies for the triplet state $^3\pi$-π^* 0-0 transition for the synthesised species in the presence of excess Gd^{3+}, and energy difference between the $^3\pi$-π^* and the Eu^{3+} $^5D_0$ or Yb^{3+} $^7F_{5/2}$ excited states.

Compound	$E_{0\text{-}0}$ ($^3\pi$-π^*) [cm^{-1}]	ΔE ($^3\pi$-π^* - $^5D_0$) [cm^{-1}]	ΔE ($^3\pi$-π^* - $^7F_{5/2}$) [cm^{-1}]
H**TzPhTpy**	21,052	3,552	10,652
H**TzPyTpy**	22,222	4,722	11,822
Me**TzPhTpy**	21,052	3,552	10,652
Me**TzPyTpy**	22,000	4,722	11,822

Table 3. Summary of the photophysical data for the sensitisation of Eu^{3+} and Yb^{3+} luminescence from diluted (*ca* 10^{-5} M) acetonitrile solutions.

		Emission (298 K)					
		λ	τ	Φ	τ_r	Φ_i	η
Compound	Ln^{3+}	[nm]	[μs]		[μs]		
H**TzPhTpy**	Eu^{3+}	618[a]	1,225	0.239	2,802	0.437	0.545
H**TzPyTpy**	Eu^{3+}	618[a]	1,194	0.208	2,749	0.434	0.478
Me**TzPhTpy**	Eu^{3+}	618[a]	1,087	0.249	2,747	0.396	0.630
Me**TzPyTpy**	Eu^{3+}	618[a]	1,263	0.214	2,806	0.450	0.476
H**TzPhTpy**	Yb^{3+}	980	10.07	-	1,200[b]	0.008	-
H**TzPyTpy**	Yb^{3+}	980	10.62	-	1,200[b]	0.009	-
Me**TzPhTpy**	Yb^{3+}	980	9.64	-	1,200[b]	0.008	-
Me**TzPyTpy**	Yb^{3+}	980	8.48	-	1,200[b]	0.007	-

[a] Only the more intense maximum belonging to the hypersensitive $^5D_0 \rightarrow {}^7F_2$ transition is reported; [b] literature value.

The addition of $[Eu(NO_3)_3(DMSO)_n]$ to acetonitrile solutions of the four species showed the typical red emission upon excitation at 310 nm. The four emission spectra are virtually superimposable, demonstrating that the Eu^{3+} complexes in solution are very similar (Figure 11).[41] The profiles are composed of the typical line-like peaks corresponding to the $^5D_0 \rightarrow {}^7F_J$ (J = 0-4) transitions. No residual fluorescent or phosphorescent emission from the ligand was observed in the spectra. The $^5D_0 \rightarrow {}^7F_0$ is visible and has a calculated full width at half maximum below 60 cm^{-1}, again supporting the fact that the emissive species have a unique and similar coordination environment.[41] The quantum yield values are in the 0.20-0.25 range. From the spectral profiles, the radiative decay (τ_r) values, reported in Table 3, can be calculated by means of the equation

$$(\tau_r)^{-1} = A_{MD,0} \times n^3 \times (I_{tot}/I_{MD})$$

where $A_{MD,0}$ is a constant of value 14.65 s^{-1}, n is the refractive index of the solvent, and I_{tot}/I_{MD} is the ratio of the integrated intensity of the whole spectrum (I_{tot}) versus the integrated intensity of the magnetic dipole transition $^5D_0 \rightarrow {}^7F_1$ (I_{MD}). From the values of τ_r, the intrinsic quantum yield (Φ_i) can be calculated as the ratio of τ/τ_r, and the sensitisation efficiency (η) as the ratio of Φ/Φ_i. The data, reported in Table 3, indicate that all the four species are good sensitisers of Eu^{3+} luminescence, with efficiencies ranging from 0.48 to 0.63. These data are consistent with previously reported luminescence properties of Eu^{3+} centres bound to terpyridine-type ligands. [11,42]

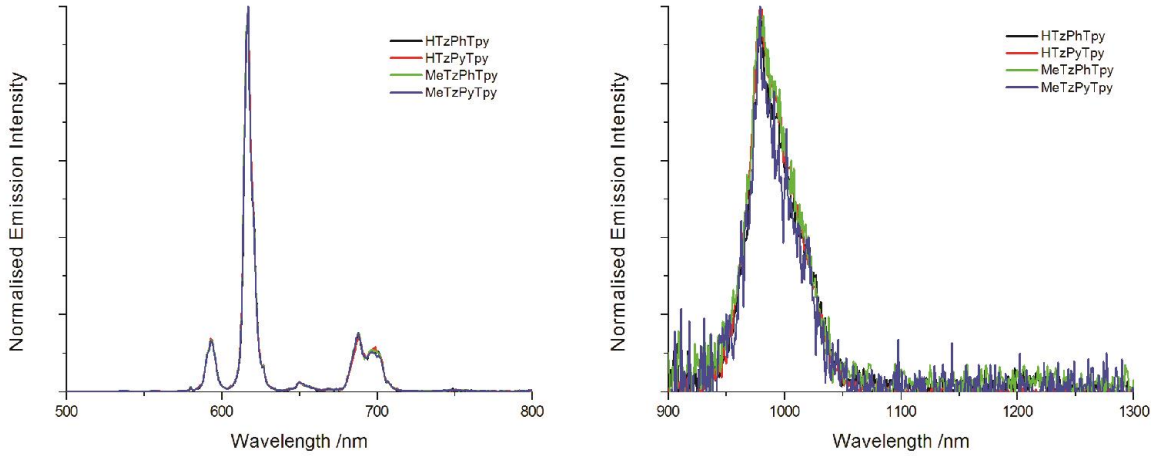

Figure 11. Emission profiles from diluted (*ca* 10^{-5} M) acetonitrile solutions of the synthesised species in the presence of excess Eu^{3+} (left) or Yb^{3+} (right), with excitation wavelength set at 310 nm.

The addition of $[Yb(NO_3)_3(DMSO)_n]$ to acetonitrile solutions of the four species also caused the quenching of the ligand-centred emission with concomitant sensitisation of the Yb^{3+} luminescence (Figure 11). A broad band in the NIR region with characteristic peak at 980 nm is evident in each case, which is ascribed to the radiative decay occurring from the $^2F_{5/2} \rightarrow {}^2F_{7/2}$ transition. The excited state lifetime decay is similar in all cases and ranges between 8.48 and 10.62 μs, which are typical values for Yb^{3+} NIR emission. From these values, and assuming a radiative decay for Yb^{3+} at 1,200 μs, the intrinsic quantum yields of these complexes can be estimated to be just below 0.01. These values are typical for Yb^{3+} complexes sensitised by terpyridine ligands.[42]

Conclusions

In this work, four new tetrazole-containing species were synthesised, characterised, and investigated in relations to their photophysical properties. The species are composed of protonated or methylated

tetrazole moieties conjugated to terpyridine functional groups, and spaced by either a phenyl or pyrdyl ring. The compounds are emissive in the UV-blue region of the spectrum and exhibit high (77-85%) to moderate quantum yields (28-32%) for the pronated and methylated species, respectively. Significant variations in the emission profiles of the methylated species could be detected upon addition of acids and bases, consistent with protonation of the terpyridine functional group causing a lowering of the HOMO-LUMO gap. The remaining protonated tetrazole species also showed variations, albeit with more complicated trends due to the added protonation site on the tetrazolate ring. The species were studied as sensors for important biological and environmental metal cations, highlighting a selective and ratiometric response to Zn^{2+} compared to other transition, alkali and alkali earth cations. Furthermore, the response of the species to the detection of Zn^{2+} could be well discriminated from Cd^{2+} cations. Lastly, the synthesised species were investigated as sensitisers for lanthanide luminescence, highlighting efficient sensitisation for red emitting Eu^{3+} and near infrared emitting Yb^{3+} cations. This work has highlighted terpyrdine-functionalised tetrazole species as very versatile molecules with useful luminescent properties and potential application in fields such as sensing and optical materials.

Experimental Section

General considerations

All reagents and solvents were purchased from Sigma Aldrich and used as received without further purification. The $[Ln(NO_3)_3(DMSO)_n]$ (Ln^{3+} = Gd^{3+}, Eu^{3+}, Yb^{3+})[37], NC**PhTpy**,[22] and NC**Py**CHO[26] precursors were prepared according to previously published procedures Nuclear magnetic resonance spectra,

consisting of 1H and 13C, were recorded using a Bruker Avance 400 spectrometer (400.1 MHz for 1H, 100 MHz for 13C) at 300 K. ^{1}H and ^{13}C chemical shifts were referenced to residual solvent signals. Infrared spectra were recorded in the solid state, using an attenuated total reflectance Perkin-Elmer Spectrum 100 FT-IR, equipped with a diamond stage. Compounds were scanned from 4000 to 650 cm^{-1}. The intensities of the IR bands are reported as strong (s), medium (m), or weak (w). Melting points were determined Using a BI Barnstead Electrothermal 9100 apparatus. Elemental analyses were obtained at the Central Science Laboratory, University of Tasmania, using a Thermo Finnigan EA 1112 Series Flash.

Photophysical measurements

Absorption spectra were recorded at room temperature using a Perkin Elmer Lambda 35 UV/Vis spectrometer. Uncorrected steady state emission and excitation spectra were recorded from air-equilibrated solutions on an Edinburgh FLSP980 spectrometer equipped with a 450 W Xenon arc lamp, double excitation and double emission monochromators and a Peltier cooled Hamamatsu R928P photomultiplier tube (185-850 nm) as well as a Hamamatsu R5509-42 photomultiplier for detection of NIR radiation (spectra range 800-1400 nm). Emission and excitation spectra were corrected for source intensity (lamp and grating) and emission spectral response (detector and grating) by a calibration curve supplied with the instrument. According to the approach described by Demas and Crosby,[43] luminescence quantum yields were measured in optically dilute solutions (O.D. < 0.1 at excitation wavelength) obtained from absorption spectra on a wavelength scale [nm] and compared to the reference emitter by the following equation:

10.1002/ejic.201700663

$$F_x = F_r \frac{\left[A_r(\lambda_r)\right]}{\left[A_x(\lambda_x)\right]} \frac{\left[I_r(\lambda_r)\right]}{\left[I_x(\lambda_x)\right]} \frac{\left[n_x^2\right]}{\left[n_r^2\right]} \frac{\left[D_x\right]}{\left[D_r\right]}$$

where *A* is the absorbance at the excitation wavelength λ, *I* is the intensity of the excitation light at the excitation wavelength λ, *n* is the refractive index of the solvent, *D* is the integrated intensity of the luminescence and Φ is the quantum yield. The subscripts *r* and *x* refer to the reference and the sample, respectively. The quantum yield determinations were performed at identical excitation wavelength for the sample and the reference, therefore cancelling the $I_r(\lambda_r)/I_x(\lambda_x)$ term in the equation. The synthesised species were measured against an air-equilibrated aqueous solution of quinine sulfate in 0.1 M H_2SO_4 used as reference (Φ_r = 0.546).[44] Emission lifetimes (τ) were determined with the time-correlated single photon counting (TCSPC) technique with the same Edinburgh FLSP920 spectrometer using pulsed picosecond LEDs (EPLED 295 or EPLED 360, FHWM < 800 ps) as the excitation source, with repetition rates between 10 kHz and 1 MHz, and the above-mentioned R928P PMT as detector. On the other hand, emission lifetimes of Ln^{3+} cations were determined with a microsecond flash-lamp as the excitation source. The goodness of fit was assessed by minimising the reduced χ^2 function and by visual inspection of the weighted residuals. The solvents used for the preparation of the solutions for photophysical investigations was of spectrometric grade. The prepared solution was filtered through a 0.2 mm syringe filter before measurement. Experimental uncertainties are estimated to be ±8% for lifetime determinations, ±20 % for quantum yields, ±2 nm and ±5 nm for absorption and emission peaks.

Synthetic details

*Synthesis of H**TzPhTpy**.* To toluene (50 mL) in an ice bath, triethylamine (0.8 mL, 5.8 mmol) and HCl (0.70 mL, 5.8 mmol) were combined and stirred until fuming subsided. NC**PhTpy** (1.93 g, 5.8 mmol) and NaN_3 (0.4 g, 5.8 mmol) were added and the mixture was stirred at reflux overnight. The solvent was evaporated under reduced pressure and the solid recrystallised from water (50 mL) and then washed with (3×20mL) DCM. Yield: 0.750 g (35 %). M.p. 280 ◦C dec. IR ν/cm^{-1}: 3046 m, 2444 m, 1683 w, 1605 w, 1593 s, 1581 s, 1542 s, 1470 m, 1393 s, 1295 w, 1113 w, 1076 w, 1008 s, 890 w, 842 w, 793 s. ^{1}H-NMR (DMSO-d_6) δ/ppm: 8.78-8.75 (4H, m), 8.66 (2H, d, J = 8.1 Hz), 8.26 (2H, d, J = 8.8 Hz), 8.02 (2H, app t, J = 8.6 Hz), 7.97 (2H, d, J = 8.4Hz), 7.54-7.49 (2H, m). ^{13}C-NMR (DMSO-d_6) δ/ppm: 160.3 ($N_4\underline{C}$), 155.7, 155.0, 149.4, 149.2, 137.4, 135.8, 133.6, 127.0, 126.7, 124.5, 120.9, 117.6. Anal. Calcd (%) for H**TzPhTpy**·0.2(H_2O): C 69.35, H 4.02, N 25.73. Found: C 69.54, H 3.85, N 25.60.

*Synthesis of H**TzPy**CHO.* To toluene (40 mL) in an ice bath, triethylamine (0.52 mL, 3.7 mmol) and HCl (0.41 mL, 3.7 mmol) were combined and stirred until fuming subsided. 2-cyanopyridine-5-carboxyalhedyde (0.5 g, 3.7 mmol) and NaN_3 (0.24 g, 3.7 mmol) were added and the mixture was stirred at reflux overnight. The mixture was extracted with water (30 mL) and the aqueous phase was acidified and the formed precipitate was filtered. The remaining aqueous solution was extracted with ethyl acetate (3x15 mL). The organic phase was collected and dried over magnesium sulfate and the solvent was removed under reduced pressure giving an off-white solid. Yield: 0.32 g (40 %). M.p. 220 ◦C dec. IR ν/cm^{-1}: 2592 m br., 1705 s, 1605 s, 1575 m, 1370 m, 1263 m, 1205 w, 1178 w, 1116 w, 1039 w, 1016 w, 845 w. ^{1}H-NMR (DMSO-d_6) δ/ppm: 10.20 (1H, s, CHO), 9.27 (1H, s), 8.50 (1H, d, J = 6.4 Hz), 8.42 (1H, d, J

= 8.2 Hz). A peak at 1.90 indicated the presence of acetic acid, probably resulting from the extraction of the acidic aqueous solution with ethyl acetate. ^{13}C-NMR (DMSO-d_6) δ/ppm: 191.8 (<u>C</u>HO), 154.6 (N_4<u>C</u>), 151.7, 147.6, 138.3, 132.3, 123.0. Anal. Calcd (%) for H**TzPy**CHO·0.1(CH_3COOH): C 47.74, H 3.00, N 38.66. Found: C 47.49, H 2.76, N 38.76.

*Synthesis of H**TzPyTpy**.* 2-acetylpyridine (0.37 mL, 3.32 mmol) was added to a solution of H**TzPy**CHO (0.2 g, 1.1 mmol) in EtOH (20 mL). KOH pellets (0.2 g, 3.3 mmol) and NH_4OH (28.0-30.0% NH_3 aqueous solution, 0.5 mL, 3.3 mmol) were then added to the solution, which was then stirred overnight at room temperature. The mixture was filtered and the solid left to dry under vacuum for 5 minutes. The solid was then dissolved in minimal water. The water was acidified to yield an off-white solid, which was filtered and dried in air. Yield: 0.13 g (40 %). M.p. 282 ◦C dec. IR ν/cm^{-1}: 3370 m, 2701 m, 1618 w, 1597 s, 1563 w, 1530 s, 1497 w, 1435 w, 1338 w, 1300 w, 1278 w, 1239 w, 1172 w, 1007 w, 993 w, 791 w. ^{1}H-NMR (DMSO-d_6) δ/ppm: 9.18 (1H, s), 8.79-8.78 (4H, m), 8.68 (2H, d, J = 8.2 Hz), 8.39 (1H, d, J = 8.2 Hz), 8.24 (1H, d, J = 8.4 Hz), 8.05 (2H, app t, J = 7.8 Hz), 7.57-7.53 (2H, m). ^{13}C-NMR (DMSO-d_6) δ/ppm: 161.1 (N_4<u>C</u>), 156.0, 155.0, 151.8, 149.5, 147.6, 146.9, 137.8, 135.3, 131.6, 124.8, 121.9, 121.2, 118.0. This compound was found to be very hygroscopic and reproducible elemental analysis could not be obtained.

*Synthesis of Me**TzPhTpy**.* H**TzPhTpy** (0.25 g, 0.66 mmol) was combined with K_2CO_3 in acetonitrile (15 mL) and stirred for 1 minute. CH_3I (44 µL, 0.66 mmol) was added and the mixture was stirred at reflux overnight. The mixture was filtered and the solvent removed under reduced pressure. The leftover solid was loaded onto Brockmann II basic alumina and eluted with DCM. The first fraction was recovered and the target compound was obtained as a white solid after removal of the solvent. Yield: 0.075 g (30 %).

M.p. 227 ◦C dec. IR ν/cm^{-1}: 3062 w, 1601 w, 1582 w, 1565 m, 1543 m, 1479 m, 1465 m, 1423 m, 1388 w, 1263 w, 1139 w, 918 w, 845. ^{1}H-NMR ($CDCl_3$) δ/ppm: 8.79 (2H, s), 8.74 (2H, d J = 8.1 Hz), 8.68 (2H, d, J = 8.1 Hz), 8.28 (2H, d, J = 8.4 Hz), 8.04 (2H, d, J = 8.4 Hz), 7.92-7.87 (2H, m, J = 2.4 Hz), 7.39-7.35 (2H, m), 5.29 (3H, s). ^{13}C-NMR ($CDCl_3$) δ/ppm: 165.0 ($N_4\underline{C}$) 156.2, 156.1, 149.5, 149.2, 140.4, 137.1, 128.0, 128.0, 127.5, 124.1, 121.6, 119.0, 39.7 ($\underline{C}H_3$). Anal. Calcd (%) for Me**TzPhTpy**·0.2(CH_2Cl_2): C 68.23, H 4.29, N 24.01. Found: C 68.27, H 3.98, N 24.14.

*Synthesis of Me**TzPyb**CHO*. H**TzPy**CHO (0.45 g, 2.5 mmol) was combined with K_2CO_3 in acetonitrile (25 mL) and stirred for 1 minute. CH_3I (0.20 mL, 3 mmol) was added and the mixture was stirred at reflux overnight. The mixture was filtered and the solvent removed under reduced pressure. The solid was loaded onto silica and eluted with a mixture of 1:1 of hexane and ethyl acetate. The first fraction was recovered and the target compound was obtained as a white solid after removal of the solvent. Yield: 0.157 g (33 %). M.p. 178-179 ◦C. IR ν/cm^{-1}: 2865, 1692 s, 1677 s, 1592 s, 1525 w, 1443 w, 1391 m, 1206 m, 1051 m, 840 m. ^{1}H-NMR ($CDCl_3$) δ/ppm: 10.18 (1H, s, C$\underline{H}$O), 9.20 (1H, s, H6), 8.41 (1H, d, J = 6.4 Hz, H3), 8.33 (1H, d, J = 6.4 Hz, H4), 4.48 (3H, s, CH_3). ^{13}C-NMR ($CDCl_3$) δ/ppm: 190.1 ($\underline{C}$HO), 164.2 (N_4C), 152.5, 151.2, 137.3, 131.9, 122.7, 40.0 ($\underline{C}H_3$). Anal. Calcd (%) for Me**TzPy**CHO·0.1($CH_3CO_2CH_2CH_3$): C 50.90, H 3.89, N 35.91. Found: C 51.27, H 3.96, N 35.65.

*Synthesis of Me**TzPyTpy**.* 2-Acetylpyridine (0.2 mL, 1.6 mmol) was added to a solution of Me**TzPy**CHO (0.15 g, 0.8 mmol) in EtOH (10 mL). KOH pellets (0.1 g, 1.8 mmol) and NH_4OH(aq) (28.0-30.0% NH_3 aqueous solution,0.24 mL, 2.2 mmol) were then added to the solution which was stirred overnight at room temperature. The mixture was filtered and the solid washed with EtOH (4 mL) and dried in air.

Yield: 0.1 g (31 %). M.p. 273 ◦C dec IR ν/cm^{-1}: 3054 w, 1603 m, 1585 s, 1566 s, 1467 s, 1440 w, 1404 s, 1120 w, 1041 w, 1015 w, 836 m. ^{1}H-NMR ($CDCl_3$) δ/ppm: 9.26 (1H, s), 8.79 (2H, s), 8.74 (2H, d, J = 4.4 Hz), 8.68 (2H, d, J = 8.2 Hz), 8.41-8.34 (2H, m), 7.92-7.88 (2H, m), 7.40-7.37 (2H, m), 4.49 (3H, s). ^{13}C-NMR ($CDCl_3$) δ/ppm: 164.8 ($N_4\underline{C}$) 156.5, 155.9, 149.3, 149.0, 147.1, 146.7, 137.2, 136.0, 135.6, 124.3, 122.5, 121.6, 119.0, 39.9 ($\underline{C}H_3$). Anal. Calcd (%) for Me**TzPyTpy**·(CH_2Cl_2): C 63.76, H 3.99, N 26.63. Found: C 63.15, H 3.47, N 26.59.

Fluorescence sensing of metal ions

The fluorescent properties of the ligands and their response to metal ions were performed for 10 μM solutions of the ligands in HEPES buffer (20 mM, pH 7.4) containing 1% DMSO (H**TzPhTpy**, H**TzPyTpy** and Me**TzPhTpy**) or 5% DMSO and 0.5% of acetic acid (Me**TzPyTpy**). To enable high throughput screening of the fluorescent response, the emission spectra for all the ligands alone and in the presence of the metal ions (10 eq) were collected on the PerkinElmer Enspire Plate Reader at the same settings (λ_{exc} = 290 nm, emission from 310 nm to 560 nm with 1 nm step size and 100 flashes per each sample).

Acknowledgments

The work was supported by the Australian Research Council (FT130100033 to MM, DP150100649 to EJN). PJW wishes to thank Curtin University for the Australian Postgraduate Award. EJN thanks the Westpac Bicentennial Foundation for a Research Fellowship.

References

[1] R. Herr, *Bioorg. Med. Chem.* **2002**, *10*, 3379–3393.
[2] G. Aromí, L. Barrios, O. Roubeau, P. Gamez, *Coord. Chem. Rev.* **2010**.
[3] C. J. McMulkin, M. Massi, F. Jones, *CrystEngComm* **2015**, *17*, 2675–2681.
[4] E. Andreiadis, R. Demadrille, D. Imbert, J. Pécaut, M. Mazzanti, *Chem. Eur. J.* **2009**, *15*, 9458–9476.
[5] S. Stagni, S. Colella, A. Palazzi, G. Valenti, S. Zacchini, F. Paolucci, M. Marcaccio, R. Q. Albuquerque, L. De Cola, *Inorg. Chem.* **2008**, *47*, 10509–10521.
[6] C. A. Strassert, C.-H. Chien, M. D. Galvez Lopez, D. Kourkoulos, D. Hertel, K. Meerholz, L. De Cola, *Angew. Chem. Int. Ed.* **2010**, *50*, 946–950.
[7] G. Koldobskii, V. Ostrovskii, *Chemistry of Heterocyclic Compounds* **1988**, *24*, 469–480.
[8] G. Koldobskii, V. Ostrovskii, B. Gidaspov, *Chemistry of Heterocyclic Compounds* **1980**, *16*, 665–674.
[9] T. Pinter, S. Jana, R. J. M. Courtemanche, F. Hof, *J. Org. Chem.* **2011**, *76*, 3733–3741.
[10] D. D'alessio, A. N. Sobolev, B. W. Skelton, R. O. Fuller, R. C. Woodward, N. A. Lengkeek, B. H. Fraser, M. Massi, M. I. Ogden, *J. Am. Chem. Soc.* **2014**, *136*, 15122–15125.
[11] M. Giraud, E. S. Andreiadis, A. S. Fisyuk, R. Demadrille, J. Pécaut, D. Imbert, M. Mazzanti, *Inorg. Chem.* **2008**, *47*, 3952–3954.
[12] S. Stagni, A. Palazzi, S. Zacchini, B. Ballarin, C. Bruno, M. Marcaccio, F. Paolucci, M. Monari, M. Carani, A. J. Bard, *Inorg. Chem.* **2006**, *45*, 695–709.
[13] D. D'alessio, S. Muzzioli, B. W. Skelton, S. Stagni, M. Massi, M. I. Ogden, *Dalton Trans.* **2012**, *41*, 4736–4739.
[14] P. J. Wright, S. Muzzioli, B. W. Skelton, P. Raiteri, J. Lee, G. Koutsantonis, D. S. Silvester, S. Stagni, M. Massi, *Dalton Trans.* **2013**, *42*, 8188–8191.
[15] P. J. Wright, S. Muzzioli, M. V. Werrett, P. Raiteri, B. W. Skelton, D. S. Silvester, S. Stagni, M. Massi, *Organometallics* **2012**, *31*, 7566–7578.
[16] M. V. Werrett, D. Chartrand, J. D. Gale, G. S. Hanan, J. G. MacLellan, M. Massi, S. Muzzioli, P. Raiteri, B. W. Skelton, M. Silberstein, et al., *Inorg. Chem.* **2011**, *50*, 1229–1241.
[17] C. Femoni, S. Muzzioli, A. Palazzi, S. Stagni, S. Zacchini, F. Monti, G. Accorsi, M. Bolognesi, N. Armaroli, M. Massi, et al., *Dalton Trans.* **2013**, *42*, 997–1010.
[18] K. D. M. MaGee, P. J. Wright, S. Muzzioli, C. M. Siedlovskas, P. Raiteri, M. V. Baker, D. H. Brown, S. Stagni, M. Massi, *Dalton Trans.* **2013**, *42*, 4233–4236.
[19] M. V. Werrett, S. Muzzioli, P. J. Wright, A. Palazzi, P. Raiteri, S. Zacchini, M. Massi, S. Stagni, *Inorg. Chem.* **2014**, *53*, 229–243.
[20] M. V. Werrett, G. S. Huff, S. Muzzioli, V. Fiorini, S. Zacchini, B. W. Skelton, A. Maggiore, J. M. Malicka, M. Cocchi, K. C. Gordon, et al., *Dalton Trans.* **2015**, *44*, 8379–8393.
[21] C. A. Bader, T. Shandala, E. A. Carter, A. Ivask, T. Guinan, S. M. Hickey, M. V. Werrett, P. J. Wright, P. V. Simpson, S. Stagni, et al., *PLoS ONE* **2016**, *11*, e0161557.
[22] J. Wang, G. S. Hanan, *Synlett* **2005**, *2005*, 1251–1254.
[23] K. Koguro, T. Oga, S. Mitsui, R. Orita, *Synthesis* **1998**, 910–914.
[24] R. Butler, V. Garvin, *J. Chem. Soc., Perkin Trans. 1* **1981**, 390–393.
[25] R. Butler, V. Garvin, H. Lumbroso, C. Liégeois, *J. Chem. Soc., Perkin Trans. 2* **1984**, 721–725.

[26] C. F. Koelsch, A. G. Whitney, *J. Org. Chem.* **1941**, *06*, 795–803.
[27] A. Downard, P. Steel, J. Steenwijk, *Aust. J. Chem.* **1995**, *48*, 1625–1642.
[28] P. J. Wright, M. G. Affleck, S. Muzzioli, B. W. Skelton, P. Raiteri, D. S. Silvester, S. Stagni, M. Massi, *Organometallics* **2013**, *32*, 3728–3737.
[29] E. J. New, *ACS Sens.* **2016**, *1*, 328–333.
[30] K. A. McCall, C. Huang, C. A. Fierke, *J. Nutr.* **2000**, *130*, 1437S–1446S.
[31] E. L. Que, R. Bleher, F. E. Duncan, B. Y. Kong, S. C. Gleber, S. Vogt, S. Chen, S. A. Garwin, A. R. Bayer, V. P. Dravid, et al., *Nature Chem.* **2014**, *7*, 130–139.
[32] K. P. Carter, A. M. Young, A. E. Palmer, *Chem. Rev.* **2014**, *114*, 4564–4601.
[33] V. Fiorini, A. M. Ranieri, S. Muzzioli, K. D. M. MaGee, S. Zacchini, N. Akabar, A. Stefan, M. I. Ogden, M. Massi, S. Stagni, *Dalton Trans.* **2015**, *44*, 20597–20608.
[34] X. Zhou, P. Li, Z. Shi, X. Tang, C. Chen, W. Liu, *Inorg. Chem.* **2012**, *51*, 9226–9231.
[35] M. Taki, in *Cadmium: From Toxicity to Essentiality* (Eds.: A. Sigel, H. Sigel, R.K. Sigel), Springer Netherlands, Dordrecht, **2012**, pp. 99–115.
[36] J. C. G. Bünzli, S. V. Eliseeva, *8.08 Photophysics of Lanthanoid Coordination Compounds*, Elsevier Ltd., **2013**.
[37] D. D'alessio, L. E. Karagiannidis, B. W. Skelton, M. Massi, M. I. Ogden, *Aust. J. Chem.* **2012**, *65*, 819–822.
[38] W. D. Horrocks, J. P. Bolender, W. D. Smith, R. M. Supkowski, *J. Am. Chem. Soc.* **1997**, *119*, 5972–5973.
[39] M. Mehlstäubl, G. S. Kottas, S. Colella, L. De Cola, *Dalton Trans.* **2008**, *102*, 2385–2388.
[40] B. L. Reid, S. Stagni, J. M. Malicka, M. Cocchi, G. S. Hanan, M. I. Ogden, M. Massi, *Chem. Commun.* **2014**, *50*, 11580–11582.
[41] K. Binnemans, *Coord. Chem. Rev.* **2015**, *295*, 1–45.
[42] A. De Bettencourt-Dias, *Dalton Trans.* **2007**, *49*, 2229–2241.
[43] J. Demas, G. Crosby, *J. Phys. Chem.* **1971**, *75*, 991–1024.
[44] D. Eaton, *Pure Appl. Chem.* **1988**, *60*, 1107–1114.

10.1002/ejic.201700663

Graphical Abstract

Luminescence pH Sensing

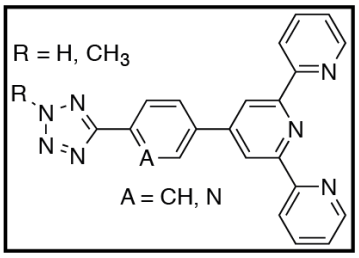

Ratiometric Zn^{2+} Sensing Lanthanide Sensitisation

Tetrazole functional groups in conjugation with terpyridine systems exhibit intrinsic luminescent properties that can exploited in areas such as pH sensing, ratiometric and efficient sensing of Zn^{2+} cations with discrimination from Cd^{2+} interference as well as sensitisation of visible and near infrared emission from lanthanide ions.